Article

A Phosphatidyl Conjugated Telomerase-Dependent Telomere-Targeting Nucleoside Demonstrates Colorectal Cancer Direct Killing and Immune Signaling

Merve Yilmaz , Sibel Goksen , Ilgen Mender , Gunes Esendagli , Sefik E. Erdener , Alessandra Ahmed , Ates K. Tenekeci , Larisa L. Birichevskaya , Sergei M. Gryaznov * , Jerry W. Shay * , Z.Gunnur Dikmen *

Posted Date: 29 September 2024

doi: 10.20944/preprints202409.2316.v1

Keywords: Cancer; Telomerase; telomere-targeted therapy; 6-thio-dG; phosphatidyl lipid conjugated 6-thio-dG

Article

A Phosphatidyl Conjugated Telomerase-Dependent Telomere-Targeting Nucleoside Demonstrates Colorectal Cancer Direct Killing and Immune Signaling

Merve Yilmaz [1,2], Sibel Goksen [3], Ilgen Mender [4], Gunes Esendagli [3,5], Sefik Evren Erdener [6], Alessandra Ahmed [2], Ates Kutay Tenekeci [1], Larisa L. Birichevskaya [4], Sergei M. Gryaznov [4,*], Jerry W. Shay [2,*] and Z.Gunnur Dikmen [1,*]

[1] Hacettepe University Faculty of Medicine, Department of Medical Biochemistry, Ankara, Turkey
[2] UT Southwestern Medical Center, Department of Cell Biology, TX, USA
[3] Hacettepe University Institute of Health Sciences, Department of Medical and Surgical Research, Ankara, Turkey
[4] MAIA Biotechnology, Inc., Chicago, IL, USA
[5] Hacettepe University, Cancer Institute, Department of Basic Oncology, Ankara, Turkey
[6] Hacettepe University Faculty of Medicine, Neurological and Psychiatric Research and Application Center, Ankara, Turkey
* Correspondence: sgryaznov@maiabiotech.com (S.M.G.); jerry.shay@utsouthwestern.edu (J.W.S.); gunnur@hacettepe.edu.tr or zgunnur@gmail.com (Z.G.D.)

Abstract: Telomerase and telomeres are crucial in cancer cell immortalization, making them key targets for anticancer therapies. Currently, 6-thio-dG combined with the anti-PD1 inhibitor Cemiplimab is under Phase 2 clinical investigation (NCT05208944) in NSCLC patients resistant to prior immunotherapies. This study presents the design, synthesis, and evaluation of novel bimodular conjugate molecules combining telomere-targeting nucleoside analogs and phosphatidyl diglyceride groups. Among them, dihexanoyl-phosphatidyl-THIO (diC6-THIO) showed high anticancer activity with sub-μM EC50 values in vitro across various cancer cell lines. In mouse colorectal cancer models, diC6-THIO demonstrated strong anticancer effects alone and in combination with PD1/PD-L1 inhibitors. Administration of this compound resulted in the efficient formation of Telomere dysfunction Induced Foci (TIFs) in vitro, indicating an on-target, telomerase-mediated telomere-modifying mechanism of action for the molecule. Systemic treatment also activated $CD4^+$ and $CD8^+$ T cells while reducing regulatory T cells, indicating immune system enhancement. These findings highlight diC6-THIO as a promising telomere-targeting prodrug with dual effects on telomere modification and immune activation.

Keywords: cancer; telomerase; telomere-targeted therapy; 6-thio-dG; phosphatidyl lipid conjugated 6-thio-dG

1. Introduction

Colorectal cancer (CRC) is the third leading cause of cancer-related deaths globally. The overall 5-year relative survival rate is 63%. In clinical settings, primary treatment options for colorectal cancer depend on the stage of the cancer and the patient's individual circumstances. Even though the options are chemotherapy, targeted therapy, radiation therapy, immunotherapy, and surgery, treatment plans can change over time based on the patient's response to therapy and disease progression [1, 2]. Three FDA-approved immune checkpoint inhibitors (ICIs) targeting programmed cell death 1 (PD-1) and cytotoxic T lymphocyte antigen 4 (CTLA-4) (Pembrolizumab, Nivolumab, Ipilimumab, respectively) are currently in clinical use for colorectal cancer [3]. Unfortunately, ICIs often provide a limited contribution to patient survival in clinical studies [4-6]. Therefore, it is crucial

 doi:10.20944/preprints202409.2316.v1

to find new therapeutic approaches and modalities to treat colorectal cancer that might also allow expanding the efficacy of the immunotherapies.

Targeted therapies, as opposed to non-specific chemotherapies, are designed to minimize adverse effects on normal tissues by targeting uniquely aberrant cancer markers. Combining targeted therapies and/or chemotherapies with prodrug strategies has shown some promises in cancer treatment [7]. Prodrugs are commonly characterized as pharmacologically inactive molecules. Nevertheless, their structural adaptability, achieved through modifications, facilitates in vivo conversion through enzymatic or chemical processes, leading to the release of bioactive agents - pharmacophores [8]. Fatty acids, cholesterol, glycerides, and phospholipids are some of the molecular entities that are used in the design of nanocarriers since they have the capability of self-assembling into nanostructures. Small molecule lipidic prodrugs provide several advantages including reported minimal toxicity, due to the endogenous fatty materials they contain, increased cellular uptake, and a better pharmacokinetic profile, [9, 10]. Due to these natural lipids being generally minimally or non-toxic, biocompatible, and biodegradable, lipid-based prodrugs emerge as attractive candidates for drug development [11-14].

Hence, we hypothesized that utilization of the hydrophobic and hydrophilic properties of diacylglycerophospholipids, may facilitate the improved solubility and cellular uptake of poorly water-soluble compounds, and could allow the development of a new class of anticancer prodrugs.

Telomeres are found at the end of eukaryotic chromosomes and are composed of repetitive nucleotide sequences TTAGGG [15, 16]. While telomeres shorten during each cell cycle in normal cells, they are elongated by the telomerase enzyme which provides an unlimited proliferative capacity to most cancer cells [17]. The nucleoside analog 6-thio-2′deoxyguanosine (known as 6-thio-dG) is modified in its 5′-triphosphate form and is effectively recognized by telomerase and consequently incorporated into newly synthesized telomeric DNA products. This telomere modification by 6-thio-dG leads to TIFs (Telomere dysfunction Induced Foci) formation, also known as telomeric DNA damage signals. Since approximately 85% of all tumors express telomerase activity [18], while the vast majority of normal untransformed cells are telomerase-negative, targeting telomerase-positive cancer cells through telomeric DNA modifications enhances anticancer treatment specificity toward cancer cells without significantly affecting normal cells [19, 20].

In this work, we designed, prepared, and evaluated a series of new phospholipid-conjugated 6-thio-dG derivatives with variable length of fatty acid residues, to assess their therapeutic effects both in vitro and in vivo models. Dihexanoyl phosphatidyl 6-thio-dG conjugate (designated as diC6-THIO) showed higher cancer cell cytotoxicity in vitro as compared to the other lipid conjugates. Therefore, we selected diC6-THIO for further in vivo evaluation as a potential candidate for advanced telomere-targeted therapies. The chemical structures of the studied phosphatidyl nucleoside conjugates are shown in Figure 1A. We conducted a series of in vitro and in vivo experiments to evaluate the therapeutic effect of diC6-THIO. These experiments confirmed the proposed mechanism of action, involving the induction of telomeric DNA damage in colorectal cancer models using the DiAna plugin methodology [21]. Following the effective dose-findings in mouse experiments, we evaluated whether diC6-THIO could activate the host innate immune system and induce adaptive immune responses in the tumor microenvironment (TME) using the flow-cytometry method. Finally, syngeneic immunocompetent CRC mouse models were used to study the anticancer effects of diC6-THIO treatment in combination with anti-PD-L1 therapy.

Preprints.org (www.preprints.org) | NOT PEER-REVIEWED | Posted: 29 September 2024 doi:10.20944/preprints202409.2316.v1

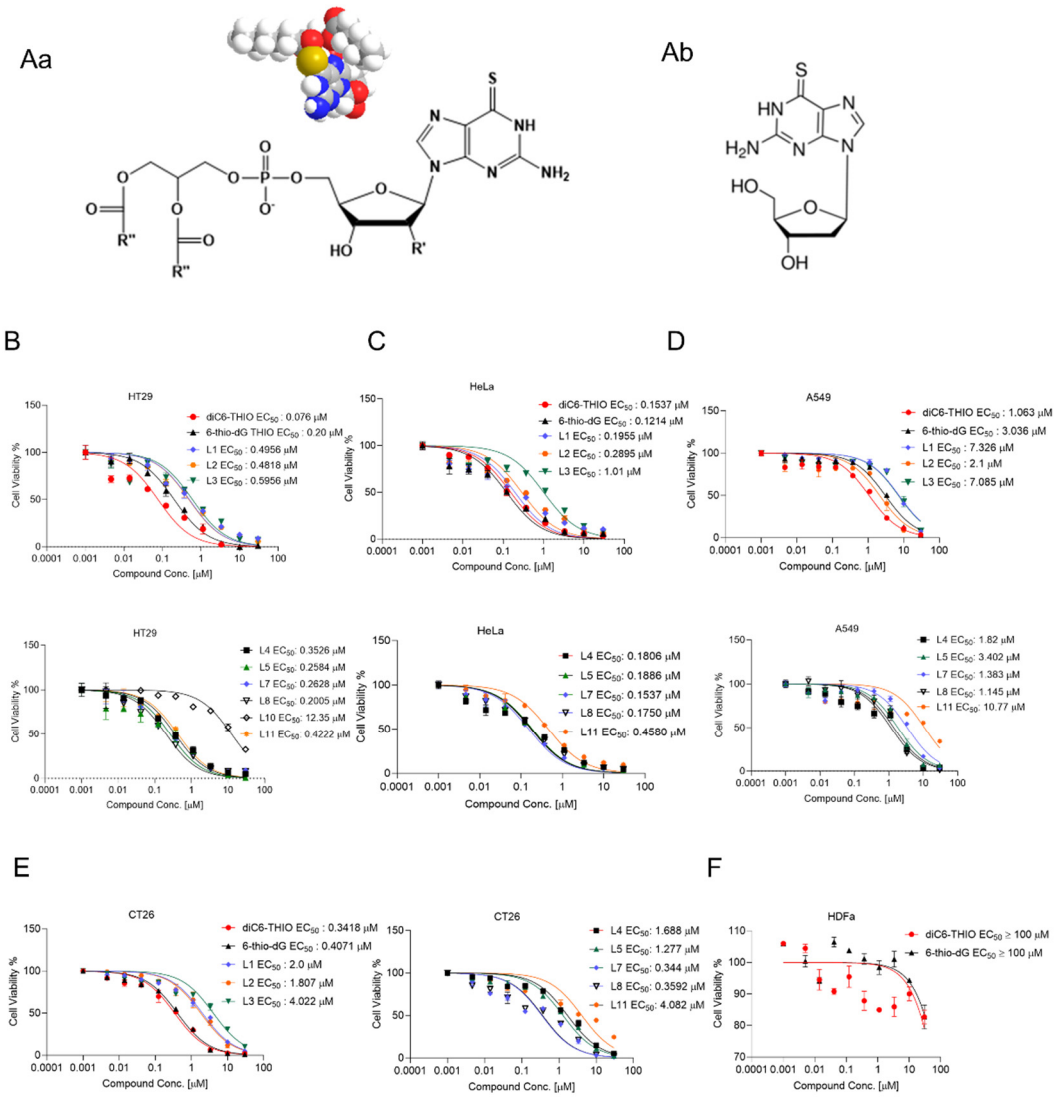

Figure 1. Biologic activity of phosphatidyl nucleoside conjugates in different human and murine cancer cell lines. General chemical structure of nucleoside phosphatidyl diglycerides, where R′ = H, and R″ = C3 - C17 fatty acid residues; for diC6-THIOmolecule R′ = H, R″ = C5 (Aa). Chemical structures of 6-thio-dG (Ab). Cell viability of human colorectal HT29 (B), human cervical HeLa (C), human NSCLC A549 (D), murine colorectal CT26 (E) cancer cell lines, and human dermal fibroblast HDFa cells (F) treated with the indicated concentrations of compounds for 4 days. Cell viability was measured using the MTT Assay. Samples were analyzed in triplicate, and EC_{50} values were calculated using GraphPad Prism.

2. Materials and Methods

Cell Lines: Human colorectal (HT29), human cervical (HeLa), human non-small cell lung cancer (A549), parental human breast cancer (MDAMB-231 WT) and its brain metastatic derivative (BrM) and bone metastatic derivative (BoM-1833), human glioblastoma (U87), murine colorectal cancer (CT26), and a human dermal fibroblast (HDFa) cell strain were purchased from the ATCC. Murine colorectal carcinoma (MC38) cells were obtained from Nanjing Cobioer Biosciences Co., Ltd. Lewis lung carcinoma (LLC) cells were obtained from the National Collection of Authenticated Cell Cultures. All cell lines were routinely evaluated using mycoplasma contamination kit (R&D). HT29 and HeLa cells were cultured in Dulbecco's Modified Eagle's Medium (DMEM) (Serena, Pessin Germany) supplemented with 10% fetal bovine serum (FBS) (Serena, Pessin Germany), A549 and CT26 cell lines were cultured in Roswell Park Memorial Institute (RPMI) 1640 medium (Serena, Pessin Germany) supplemented with 10% FBS (Serena, Pessin Germany), MDAMB-231, BrM and

 doi:10.20944/preprints202409.2316.v1

BoM-1833 cell lines were cultured in Media X with 10% FBS, HDFa cells were cultured in 1:1 mixture of DMEM and Ham's F-12. supplemented with 15% heat-inactivated FBS, 100 Unit/milliliter (U/ml) penicillin (Serena, Pessin Germany) 1% L-glutamine (Serena, Pessin Germany), MC38 and LLC cells were maintained in DMEM medium supplemented with 10% FBS. All cell lines were incubated under 5% CO_2 at 37°C.

Drug Preparation: Anti-mouse PD-L1 was purchased from BioCell (#BE0101; New Hampshire, Lebanon), anti-mouse PD1 antibody was purchased from BioXCell (#BE0146); 6-thio-dG and other phosphatidyl nucleoside conjugate compounds were supplied by MAIA Biotechnology (Chicago, USA). For in vitro experiments, 6-thio-dG and other compounds were dissolved in 100% dimethyl sulfoxide (DMSO) (Merck, Darmstadt, Germany) to prepare stock solutions at 5 mM and 30 mM concentrations, respectively; it was stored at -20°C. For in vivo experiments, 6-thio-dG (3 milligrams/kilogram; mg/kg) and diC6-THIO (3 mg/kg) were prepared in the mixture of 5% DMSO and 95% PBS for intraperitoneal(i.p.) or diC6-THIO (6 mg/kg) and sdiC6-THIO (6 mg/kg) was prepared in PBS for intravenous administration (i.v.). The anti-PD-L1 antibody (10F.9G2) was prepared at a concentration of 2.6mg/mL (Bio X Cell, USA) in PBS; 6-thio-dG, diC6-THIO, anti-PD-L1 and anti-PD1 agents were stored at 4°C. The anti-PD1 antibody (clone: RMP1-14) was prepared at a concentration of 1 mg/mL in PBS and stored at 4°C.

Cell Viability Assay: To assess the half-maximal effective concentration (EC_{50}) of compounds, both murine and human cancer cell lines were screened with 6-thio-dG and candidate compounds with a 3-fold dilution series in 9 different points in 96-well plates. Cells were seeded 24 hours before drug treatment and analyzed using the CellTiter Glo, MTT assay (1 milligram/milliliter; mg/ml per cell) (Naturewill Biotechnology, Sichuan, China) or Cell Counting Kit-8 (CCK8) after 4-day incubation. The cell counts per well varied between 1000 and 5000 cells according to their doubling times. Dose-response curves and EC_{50} values were generated using the GraphPad Prism software. Samples were analyzed in triplicate, and the standard deviations were derived from a minimum of three independent experiments.

Droplet Digital TRAP (ddTRAP): To measure the telomerase activity, cell pellets were prepared according to the ddTRAP protocol [22]. Briefly, cells were cultured to the desired density, counted (50,000 to 1 × 10^6 cells), and pelleted. The pellets were either lysed immediately on ice or flash-frozen in liquid nitrogen and stored at −80°C. Lysis was performed in 40 µl of NP-40 buffer for 30 minutes on ice. The lysate cell number equivalent was calculated by dividing the number of cells lysed by the volume of lysis buffer. One microliter of lysate was added to a 50 µl extension reaction containing 1X TRAP reaction buffer, 0.4 mg/ml BSA, 200 nM TS telomerase substrate, dNTPs, and incubated at 25°C for 40 minutes, followed by inactivation at 95°C for 5 minutes. The ddPCR reaction was prepared with 1X EvaGreen ddPCR Supermix v2.0, 50 nM TS and ACX primers, ≤50 cell equivalents of extension product, and dH_2O to 20 µl. Droplets were generated using a droplet generator and transferred to a 96-well PCR plate. PCR was performed with a ramp rate of 2.5°C/s, including 40 cycles of 95°C for 30 s, 54°C for 30 s, and 72°C for 30 s, followed by a final hold at 4°C. Fluorescence was read using the 6-Fam channel on a droplet reader, analyzing an average of 17,000 droplets per 20 µl PCR. Telomerase activity was quantified as the number of extended TS molecules per microliter and normalized to cell equivalents. Background signal was assessed using a no-template control.

Telomere Dysfunction Induced Foci (TIF) Assay: HT29, HeLa and CT26 cells were seeded into poly-lysine (Sigma, USA) coated wells. The cells were treated with 1 µM 6-thio-dG and 1 µM diC6-THIO for 96 hours. The glass coverslips were washed with pre-extraction buffer (20 millimolar; mM Tris-HCl pH: 8; BioShop, Canada, 50 mM NaCl, 3 mM $MgCl_2$; Sigma, Germany, 0.5% Triton X-100; BioShop Canada, 300 mM sucrose; Merck, Germany) and fixed in a solution containing 4% formaldehyde (Thermo Fisher, USA). Then, the cells were permeabilized in a 0.5% solution of PBST (Triton X-100, BioShop Canada) and blocked with a 5% bovine serum albumin (BSA, Pessin, Germany) solution. The cells were incubated with the primary antibody (1:500, gammaH2AX, Cell Signaling, USA) and washed with 0.1% PBST. Subsequently, the cells were incubated with AlexaFluor 568 conjugated goat anti-mouse antibody (Invitrogen, USA), at a dilution of 1:1000 and fixed by 4% formaldehyde in PBS (Sigma, USA) at room temperature. The slides were dehydrated

 doi:10.20944/preprints202409.2316.v1

with ethanol (Sigma, Germany) solutions of 70%, 90%, 100%, and the slides were denaturated with hybridization buffer containing a peptide nucleic acid (PNA, Eurogentec, Belgium), conjugated with fluorescein amidite (FAM). The samples were heated at 85°C on a heat block for 4 minutes, washed with a washing solution (1M Tris HCl pH: 7.5, 50% formamide; Sigma, Germany, 10% BSA) and mounted using Vectashield mounting medium with DAPI (Vector Laboratories, CA, USA).

TIF images were captured using a confocal microscope (Leica, sp8) with an oil-immersion objective (63X, NA:1.4). For each region of interest, 50x50 μm^2 areas were scanned at 512x512 pixel resolution and Z-stacks with 0.3 μm steps were recorded capturing the entire axial range of the cells to be analyzed. This raw data was further processed using ImageJ/FIJI (Version: 1.54b) and background subtraction and a gaussian filter with sigma=1 pixel was applied. Quantitative analysis on these preprocessed images was then performed using DiAna plugin [21] for testing object-based 3D colocalization between green and red channels. The threshold for maxima selection was set by the user and was readjusted by manually checking the segmentation results with the raw fluorescent image data, confirming that no artificial seeds were generated and at least 90% of the visible fluorescent foci are recognized as seed maxima. Once segmentation was complete for both channels, co-localization was determined by the detection of overlapping objects, and co-localizing object volumes were calculated for each pair of objects. The statistical significance of co-localization was calculated by comparing the experimental results with a random distribution, using the respective function of the DiAna plugin. The cumulative distribution of the mean distances between objects for experimental images and randomly shuffled images were compared and the colocalizations were considered statistically significant if the experimental mean distance distribution curve was localized outside the 95% confidence interval of the randomized distance. Only statistically significant co-localization analyses are reported in the experimental results.

Radiation Therapy Experiments: HT29 cells (4000 cells/well) were seeded into 6-well plates (Nest, CA, USA) and treated with diC6-THIO (0.3 μM) and 6-thio-dG (0.3 μM) over a 96-hour incubation period. After diC6-THIOand 6-thio-dG incubation, cells were irradiated with the Varian DHX linear accelerator (Varian, MA, USA) operating at 6 MV X-ray energy, with doses of 2 Gray (Gy) and 4 Gy. Following the irradiation, the cells were cultured for an additional 24 hours and subsequently counted using methylene blue staining.

Spheroids Culture: CT26 spheroids were generated by free-floating spheroid culture system on PETG Erlenmeyer flasks in RPMI-1640 media. Single-cell suspensions were seeded into flasks as 5×10^5 cells/mL and cultivated for 5 days. After checking and confirming the spheroid formation on microscope, 1 μM and 3 μM diC6-THIO was added into the media and incubated for 96 hours.

Flow Cytometry Analysis for Spheroid Formation: Flow cytometry was used to quantify the percentage of cell viability in CT26 spheroid cells treated with diC6-THIO compared to control group. For each condition, 5 mL from the 25 mL cell/media solution was taken and centrifuged at 1000 g for 5 minutes. Supernatant was discarded and 1 mL of Trypsin-EDTA (0.05%) was added to the cell pellet, incubated for 5 minutes at 37°C. After the incubation, the trypsin solution was diluted 1:10 with base media. Single-cell suspension was verified under the microscope. Cells centrifugated again at 1000 g for 5 minutes. The supernatant was removed, cells were washed twice with FACS Buffer (PBS + 3% FBS), and centrifugated at 1000 g for 5 minutes each time. The supernatant was discarded and cells stained with eBioscience Fixable Viability Dye eFluor 506 (Ref: 65-0866-14) at a 1:50 dilution in FACS Buffer and incubated for 30 minutes at 4°C. After incubation, 1 mL of FACS Buffer was added to dilute the dye and centrifuged at 1000 g for 5 minutes. The supernatant was removed, and cells washed twice with FACS Buffer, centrifugated at 1000 g for 5 minutes. Finally, the cell pellet was resuspended in 200 μL of FACS Buffer and analyzed on the flow cytometer (Beckman CytoFLEX). Sample concentration adjusted as needed to maintain a flow rate of no more than 2500 events/minute. FSC (Forward Scatter) and SSC (Side Scatter) parameters are used to analyze and distinguish different cell populations based on their size and granularity.

In vivo Experiments: Male Nude CD1 and BALB/c mice were purchased from Kobay Experimental Animal Laboratory. All mice were maintained under specific pathogen-free conditions. This study was approved by the Ethical Committee of the Kobay Experimental Animal Laboratory

 doi:10.20944/preprints202409.2316.v1

under protocol number 603. C57BL/6N female mice (6-9 weeks old) were purchased from Beijing Vital River Laboratory Animal Technology Co., Ltd. C57BL/6N animals were housed at HitGen Inc. animal house facility.

Xenograft Mouse Tumor Model: To determine the optimal dose of diC6-THIO, $2x10^6$ human HT29 cells were injected into the right dorsal flanks of the six to eight weeks old male CD1 Nude mice in 100 µL PBS. Tumor size measurements were conducted on a weekly basis, and treatment was started when the tumor volume reached 70-100 mm^3. The mice were subjected to diC6-THIO treatment at dosages of 3 mg/kg (total of 6 doses on days 0, 2, 4, 6, 8, 10, with day 0 designated as the day of treatment start) and 6 mg/kg (total of 4 doses on days 0, 2, 4, 6, with day 0 designated as the day of treatment start). Tumor volumes were measured using a caliper by the length (a), width (b) and height (h) and calculated as tumor volume = a x b x h / 2.

Syngeneic Mouse Tumor Model: A total of $2x10^6$ murine CT26 cells were injected into the left dorsal flanks of the six to eight weeks old male BALB/c mice in 100 µL PBS with 10% Matrigel (Corning). Tumor size measurements were conducted on a weekly basis, and treatment was started when the tumor volume reached 70-100 mm^3 and designated here as day 0. In CT26 model, tumor volumes were measured using a caliper by the length (a), width (b), and height (h) and calculated as tumor volume = a x b x h / 2. When tumor volumes reached 70-100 mm^3, the animals were divided into 3 treatment groups. In the diC6-THIO treatment group, the mice were administered with 3 mg/kg diC6-THIO twice a week over 2 weeks on days 0, 2, 7, and 9 with day 0 designated as the day of treatment start. In the anti-PD-L1 group, mice were administered weekly with 10 mg/kg anti-PD-L1 for two weeks on days 4 and 11. In the sequential therapy group, mice received diC6-THIO at a dosage of 3 mg/kg, twice weekly, over 2 weeks, coupled with a weekly administration of 10 mg/kg anti-PD-L1 (diC6-THIO on days 0, 2, 7, and 9 and anti-PD-L1 on days 4, 11). Following 2 weeks of treatment mice were euthanized, and tumors were removed and analyzed by flow cytometry.

A total of $4x10^4$ murine MC38 or $2x10^6$ LLC cells were subcutaneously injected into the right dorsal flanks of the female C57BL/6N mice in 100 µl PBS (n=8 per each group). Treatment started when the tumor volume reached 70-100 mm^3 and designated as day 0. In the treatment groups, the mice were administered with 6 mg/kg diC6-THIO (i.v.) or 6 mg/kg sdiC6-THIO (i.v.) on days 0, 1, 2, 7, 8, 9 and/or 10mg/kg anti-PD1 (i.p.) on days 4 and 12. In MC38 and LLC models, tumor length and width were measured using a caliper. Tumor volume = $0.5 \times (\text{length} \times \text{width}^2)$

Flow Cytometry Analysis: Freshly collected tumor tissues were submerged in RPMI-1640 medium supplemented with 10% FBS. Mechanical fragmentation was performed with scalpel. To obtain cell suspensions following mechanical fragmentation, a sterile strainer with a pore size of 40 µm was used, and subsequently rinsed with RPMI-1640 medium supplemented with 10% FBS and centrifugated 5 min at 2000 rpm. The cells were labeled with various combinations of specific surface markers for myeloid and T cells, including CD45-PerCP (Biolegend, USA), CD11b-APC/Cy7 (Sony Biotechnology, USA), F4/80-FITC (Biolegend, USA), Gr1-PE (Biolegend, USA), CD3-BV421 (Biolegend, USA), CD4-FITC (Biolegend, USA), CD8a-PE (Biolegend, USA), CD62L-APC (Biolegend, USA), FoxP3-PE (Biolegend, USA) monoclonal antibodies for immunophenotyping. Intracellular staining of FoxP3 was performed with True-Nuclear Transcription Factor Buffer Set (Biolegend, USA) according to the manufacturer's instructions. Following the incubation with specific antibodies, the cells were washed, and the analyses were performed on a flow-cytometry (FACSCanto II, BD). The percentage values were determined according to the autofluorescence.

diC6-THIO Anti-PD-L1 and Sequential Therapy Effects on Liver and Kidney Functions: To determine whether diC6-THIO, anti-PD-L1 and sequential therapy has toxic effect on liver and kidney, we collected blood samples from treatment groups and controls, centrifuged at 2000 g for 10 minutes (Thermo Scientific, Megafuge 40R). Serum samples were used for aspartate amino transferase (AST), alanine amino transferase (ALT), creatinine and blood urea nitrogen (BUN) measurement (Beckman Coulter, AU680, USA).

Quantification and Statistical Analysis: All the data analyses were performed with GraphPad Prism 8 and presented as mean ± SEM. For flowcytometry analysis were performed with Flowjo. *p* value determined by two-way ANOVA for xenograft and syngeneic mouse model tumor growth

 doi:10.20944/preprints202409.2316.v1

experiments. Two-way ANOVA multiple comparisons were used for TIF and global DNA damage assays. For flow-cytometry analysis, the distribution of the groups was evaluated with the unpaired student t-test. In the radiation experiment and liver, and kidney function tests, the *p* value was determined by unpaired t-test. $p \leq 0.05$ was considered statistically significant.

3. Results

Screening of Phosphatidyl Conjugated Compounds in Different Cancer Cell Lines

To determine which fatty acid residues of glycerophospholipids provide the highest anticancer activity in vitro, we evaluated a series of phospholipid-conjugated compounds using HT29, HeLa, A549, CT26, MC38, LLC, HDFa, MDAMB-231 WT, BrM and BoM-1833 and U87 cells. The chemical structures of diC6-THIO and 6-thio-dG are shown in Figures 1Aa and 1Ab, respectively. We found the corresponding EC50 values to be 0.2 μM, 0.49 μM, 0.48 μM, 0.59 μM, 0.35 μM, 0.25 μM, 0.076 μM, 0.26 μM, 0.20 μM, 12.35 μM, 0.42 μM for 6-thio-dG, L1, L2, L3, L4, L5, L6 (diC6-THIO), L7, L8, L10, and L11, respectively, in HT29 cells (Figure 1B-E). We found that other phospholipid-conjugated molecules also show efficacy like diC6-THIO in these cancer cell lines (summarized in Table 1), and thus may potentially be evaluated as a second-generation of telomerase-mediated telomere-targeted candidate molecules in future preclinical studies. Consequently, we continued our preclinical studies with the most active molecule, diC6-THIO, and compared the compound's in vitro activity against 6-thio-dG. We found that the tested telomerase-positive cancer cells were sensitive to both diC6-THIO (EC50 values: 0.076 – 3.527 μM) and 6-thio-dG (EC50 values: 0.12 - 3.036 μM) (Table 1). However, diC6-THIO showed higher cytotoxicity in HT29 and A549 cancer cells as compared to 6-thio-dG (Figure 1B-D). Furthermore, we evaluated the effects of these compounds on the metastatic cell lines BrM, and BoM-1833, and compared the results with their parental MDAMB-231 cell line. Our findings indicate that both metastatic cancer cell lines, BrM and BoM-1833, are more sensitive to 6-thio-dG compared to their respective parental cell line. Additionally, the BoM-1833 metastatic cell line shows enhanced sensitivity to diC6-THIO relative to the parental MDA-MB-231 cells (Supplementary Figure S7C). At the same time, EC_{50} values for both diC6-THIO and 6-thio-dG were above 100 μM in telomerase-negative normal human dermal fibroblast cells (HDFa) (Figure 1F), demonstrating the specificity of both compounds to telomerase-positive cancer cells versus their normal untransformed counterparts.

Table 1. Summarizing the EC_{50} values of all compounds evaluated in different cell lines following a 4-day treatment.

	EC_{50} (μM)							
Compounds	**HT29**	**HeLa**	**A549**	**CT26**	**MC38**	**LLC**	**HDFa**	**U87**
6-thio-dG	0.2	0.1214	3.036	0.4071	1.507	0.172	>100	0.8985
L1	0.4956	0.1955	7.326	2	-	-	-	-
L2	0.4818	0.2895	2.1	1.807	-	-	-	-
L3	0.5956	1.01	7.085	4.022	-	-	-	-
L4	0.3526	0.186	1.82	1.688	-	-	-	-
L5	0.2584	0.1886	3.402	1.277	-	-	-	-
L6 (diC6-THIO)	0.076	0.1537	1.063	0.3418	3.527	0.3418	>100	0.7878
sdiC6-THIO	-	-	-	-	> 50	23.94	-	-
L7	0.2628	0.1537	1.383	0.344	-	-	-	-
L8	0.2	0.175	1.145	0.3592	-	-	-	-
L10	12.35	-	-	43.07	-	-	-	-
L11	0.4222	0.458	10.77	4.02	-	-	-	-

Metastatic Cell Sensitivity to diC6-THIO Correlates with Increased Telomerase Activity

 doi:10.20944/preprints202409.2316.v1

diC6-THIO is incorporated into de novo synthesized telomeres by telomerase. To assess this mechanism and correlate EC_{50} values with telomerase activity in metastatic cell lines, we performed the ddTRAP assay. Our results showed that the parental MDAMB-231 cell line exhibited lower telomerase activity compared to its metastatic derivatives (Supplementary Figure S7C). These findings suggest that the enhanced sensitivity of BoM-1833 to diC6-THIO is associated with elevated telomerase activity.

diC6-THIO Treatment Induces Telomere Dysfunction Induced Foci (TIF) Formation

To evaluate whether the diC6-THIO compound induces telomere damage in cancer cells, we treated HT29, HeLa, and CT26 cells with diC6-THIO and 6-thio-dG at 1 μM concentration for 96 hours. Co-localization of signals derived from genomic, and telomeric DNA damage foci was determined by the detection of overlapping objects (Supplementary Figure S1A (left)). These data showed that the segmentation tools exclude some spots that are not relevant to the TIF foci and capture co-localization areas (Supplementary Figure S1A (right)). In addition to co-localization measurements, DiAna technique [21] provided detectable objects in the respective images (Supplementary Figure S1B). The DiAna plugin algorithm generates a graphical representation of the cumulative distribution of the minimum center-to-center distances between objects in two different images (images for gammaH2AX and telomeres) as illustrated in Supplementary Figure S1C. Within the graphs, the blue curves correspond to the distribution observed in the experimental images. The green curves represent the confidence interval centered around the mean. Meanwhile, the red curve shows the mean distribution of the distances between objects from the experimental images and images obtained through the shuffle procedure. Significantly, the experimental blue curve lies beyond the 95% confidence interval (green) of the distance analysis following randomization. Hence, this co-localization analysis is considered statistically significant. Both 6-thio-dG and diC6-THIO induced a considerable number of telomere damage (TIFs) in all three cell lines evaluated. At the same time, treatment with diC6-THIO generated a significantly higher number of TIFs compared to 6-thio-dG in both HT29 and CT26 cancer cells (Figure 2A and B). The increase in the number of TIFs may be attributed to the presence of dihaxanoyl phosphatidyl group in the diC6-THIO structure, providing for a better cellular uptake of the molecule in HT29 and CT26 colorectal cancer cells and affecting intracellular pharmacophore's metabolism and distribution. However, no significant difference in TIFs induction was observed between diC6-THIO and 6-thio-dG in HeLa ovarian cancer cells, where the compounds' EC_{50} values were also comparable to each other (Figure 2B).

 doi:10.20944/preprints202409.2316.v1

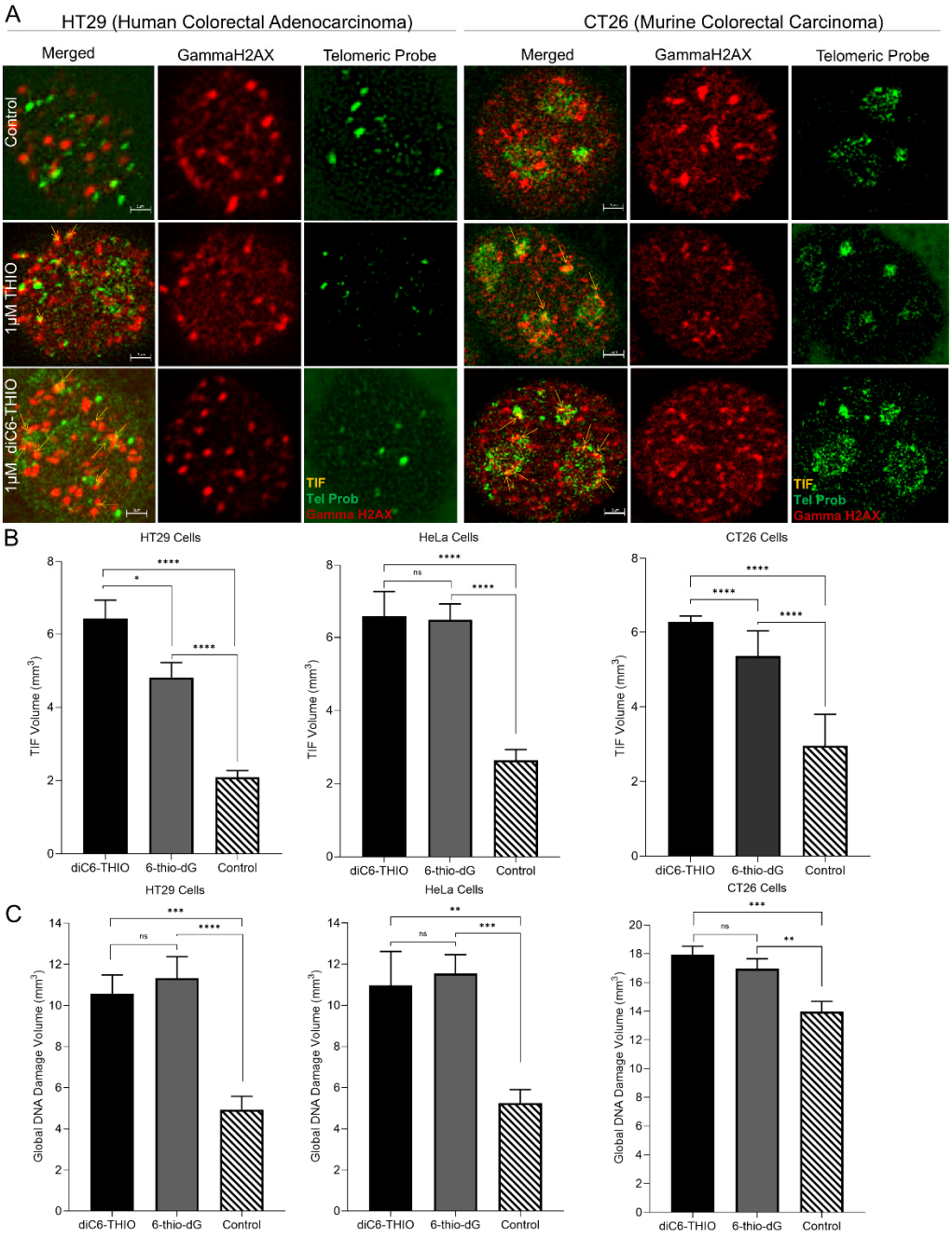

Figure 2. diC6-THIOinduces more TIFs compared to 6-thio-dG. Representative 2D images of TIF and DNA damage foci for diC6-THIO and 6-thio-dG in HT29 and CT26 cells with 1μM treatment for 4 days. Green: Telomeric probe, red: gammaH2AX and yellow: TIFs (A). Merged images with arrows show the representative pictures of TIFs (A), the quantitative measurements of TIF volumes (B) and global DNA damage (C) of HT29, HeLa and CT26 cells treated with diC6-THIO (1μM) and 6-thio-dG (1μM) for 4 days. Data are shown as means ± SEM from two to three independent experiments. *p* value was determined by two-way ANOVA followed by post-hoc test (Tukey's). All TIF and global DNA damage volumes were scored by DiAna plugging (n≈50 for HT29, HeLa, CT26 cells). *p* values for TIF between control vs 6-thio-dG (****p<0.0001) or control vs diC6-THIO(****p<0.0001) or 6-thio-dG vs diC6-THIO (*p=0.0147) in HT29, control vs 6-thio-dG (****p<0.0001) or control vs diC6-THIO (****p<0.0001) or 6-thio-dG vs diC6-THIO (p=0.9966) in HeLa, control vs 6-thio-dG (****p<0.0001) or control vs diC6-THIO (****p<0.0001) or 6-thio-dG vs diC6-THIO (****p<0.0001) in CT26. ns, not significant. *P* values for global DNA damage between control vs 6-thio-dG (****p<0.0001) or control vs diC6-THIO (***p=0.0002) or 6-thio-dG vs diC6-THIO (p = 0.8243) in HT29, control vs 6-thio-dG (***p=0.0004) or control vs diC6-THIO (**p=0.0014) or 6-thio-dG vs diC6-THIO (p=0.9314) in HeLa,

 doi:10.20944/preprints202409.2316.v1

control vs 6-thio-dG (**p=0.0077) or control vs diC6-THIO (***p=0.0003) or 6-thio-dG vs diC6-THIO (p=0.5879) in CT26. ns, not significant.

In addition, both diC6-THIO and 6-thio-dG induced global genomic DNA damage (as assessed by induction of gammaH2AX DNA damage foci) in HT29, HeLa, and CT26 cells, where there was no significant difference between diC6-THIO and 6-thio-dG treatment groups (Figure 2C). Our findings indicate that diC6-THIO exhibits higher TIFs induction than that of 6-thio-dG in colorectal cancer cells, and thereby higher degree of telomere alteration resulting in an increased activity in vitro.

diC6-THIO-Induced Dissociation of CT26 Spheroids

Sphere culture, which facilitates the entrapment and enrichment of cancer stem cells (CSCs), is widely regarded as a highly effective method for isolating CSCs from cancer cell lines and solid tumors [23, 24]. Additionally, spheroid cultures provide an optimal platform for routine assessment of toxicity and drug efficacy, facilitating the determination of safe exposure doses in well-established cellular models [25, 26]. We aim to investigate the impact of diC6-THIO on spheroid formation. Our results demonstrated that CT26 cell-derived spheroids were sensitive to diC6-THIO treatment, leading to their dissociation (Supplementary Figure S7D). This dissociation suggests that diC6-THIO may disrupt intercellular adhesion and potentially enhance the efficacy of other therapeutic modalities.

diC6-THIO Reduces Tumor Growth in HT29-Derived Xenograft and CT26 Syngeneic Mouse Models

We have previously shown that 6-thio-dG controls tumor growth with daily or every other day treatment for over 10 days in xenograft immunodeficient mice cancer models [27]. Here, we evaluated the treatment of the diC6-THIO compound in CD1 nude male mice at 3mg/kg and 6mg/kg doses, where the compound injections were done intraperitoneal, (i.p) every other day for 6-10 days. Although 6mg/kg dose resulted in animal weight loss after 4 administrations, 3mg/kg dose was well tolerated. We thus extended the treatment period with 3 mg/kg doses of diC6-THIO for up to 6 injections. Significant tumor reduction was observed both in 3mg/kg and 6mg/kg dose groups when compared to the control group (Figure 3A). These results led us to identify the 3mg/kg dose as the optimal therapeutic dose level for the following in vivo studies. Then we evaluated diC6-THIO at 3mg/kg dose level in a CT26-derived immunocompetent syngeneic mouse model of colorectal cancer. CT26 cells were inoculated into BALB/c mice and 14 days after inoculation (when the tumor volume reached ~70-100 mm^3), diC6-THIO (3mg/kg) was administered twice a week for 2 weeks (on days 0, 2, 7, and 9 with day 0 corresponds to the day of the treatment initiation). Tumor volumes were monitored and measured for 2 weeks. We observed that tumor growth was significantly reduced in the CT26-derived immunocompetent model by the treatment with diC6-THIO, without any significant animal weight loss (Figure 3B-D).

 doi:10.20944/preprints202409.2316.v1

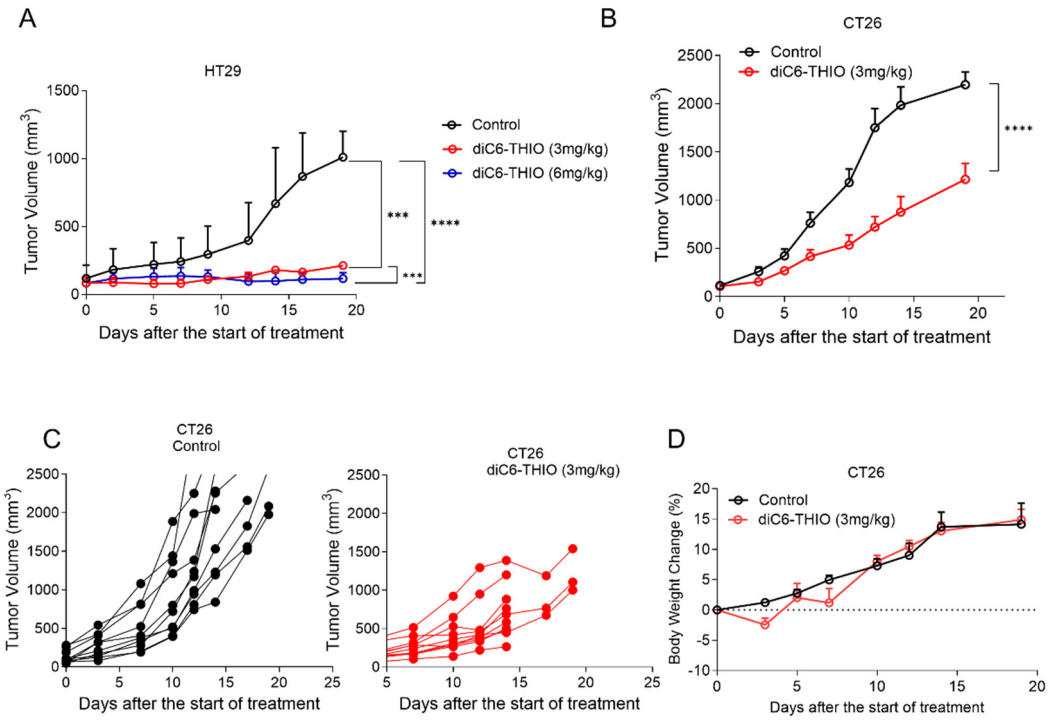

Figure 3. diC6-THIO reduces tumor growth in xenograft and syngeneic mouse models. Xenograft model with HT29 cells. The mice were subjected to 3 mg/kg diC6-THIO treatment (total of 6 doses on days 0, 2, 4, 6, 8, 10, with day 0 designated as the day of treatment start) and 6 mg/kg diC6-THIO treatment (total of 4 doses on days 0, 2, 4, 6, with day 0 designated as the day of treatment start). Tumor volumes were scored by GraphPad Prism (n=2 per each group for nude CD1 mice, $2x10^6$ HT29 cells were injected). ***p=0.0003 (control vs 3mg/kg diC6-THIO), ****p<0.0001 (control vs 6mg/kg diC6-THIO), ***p=0.0008 (3mg/kg diC6-THIO vs 6mg/kg) in two-way ANOVA, (control; untreated) (A). The BALB/c mice tumor volume measurements. $2x10^6$ murine CT26 cells were injected. BALB/c mice bearing CT26 tumors were treated with diC6-THIO (3mg/kg, days 0, 2, 7, and 9 with day 0 designated as the day of treatment start). Data are shown as means ± SEM from two independent experiments. p value was determined by two-way ANOVA by using GraphPad Prism. (n=10 per each group, ****p<0.0001 control vs diC6-THIO in two-way ANOVA, control; untreated) (B). Individual tumor growth of control and diC6-THIO treatment groups (C). Graph shows body weight changes of mice in percentage following diC6-THIO treatment. The weights were measured every 2 days (D).

diC6-THIO Treatment Enhances Activated $CD4^+$ and $CD8^+$ T Cells and Decreases T Regulatory Cells in the Tumor Microenvironment

We conducted a flow-cytometry analysis to distinguish the immune cell populations in the tumor microenvironment (Supplementary Figure S2A,B and Supplementary Figure S3A-F). The analysis showed significant change in the percentage of infiltrating immune cell populations within the tumor microenvironment in the diC6-THIO treated group compared to the control group Figure 4A and B. diC6-THIO treatment led to an elevation in total leukocyte cells within the tumor tissue (Figure 4A), predominantly composed of myeloid cells (Figure 4B). Among myeloid populations, macrophages and monocytes exhibited an increased infiltration (Figure 4C, D), while granulocyte levels remained unchanged (Figure 4E). Furthermore, there was an increase in both T helper ($CD4^+$) and cytotoxic T cell ($CD8^+$) populations, with increased numbers of activated lymphocytes in both T cell subtypes (Figure 4F, G, I, J) and a concomitant reduction in T regulatory (Treg) cells (Figure 4H). The ratio of $CD8^+$ T cells to Tregs ($CD4^+$ $FoxP3^+$), which favors T cell activity, increased with diC6-THIO treatment (Figure 4K). However, the reduction in Tregs, the trend in elevation in cytotoxic and activated $CD8^+$ T cells and the increased ratio of cytotoxic T cells to Tregs with treatment were not statistically significant.

 doi:10.20944/preprints202409.2316.v1

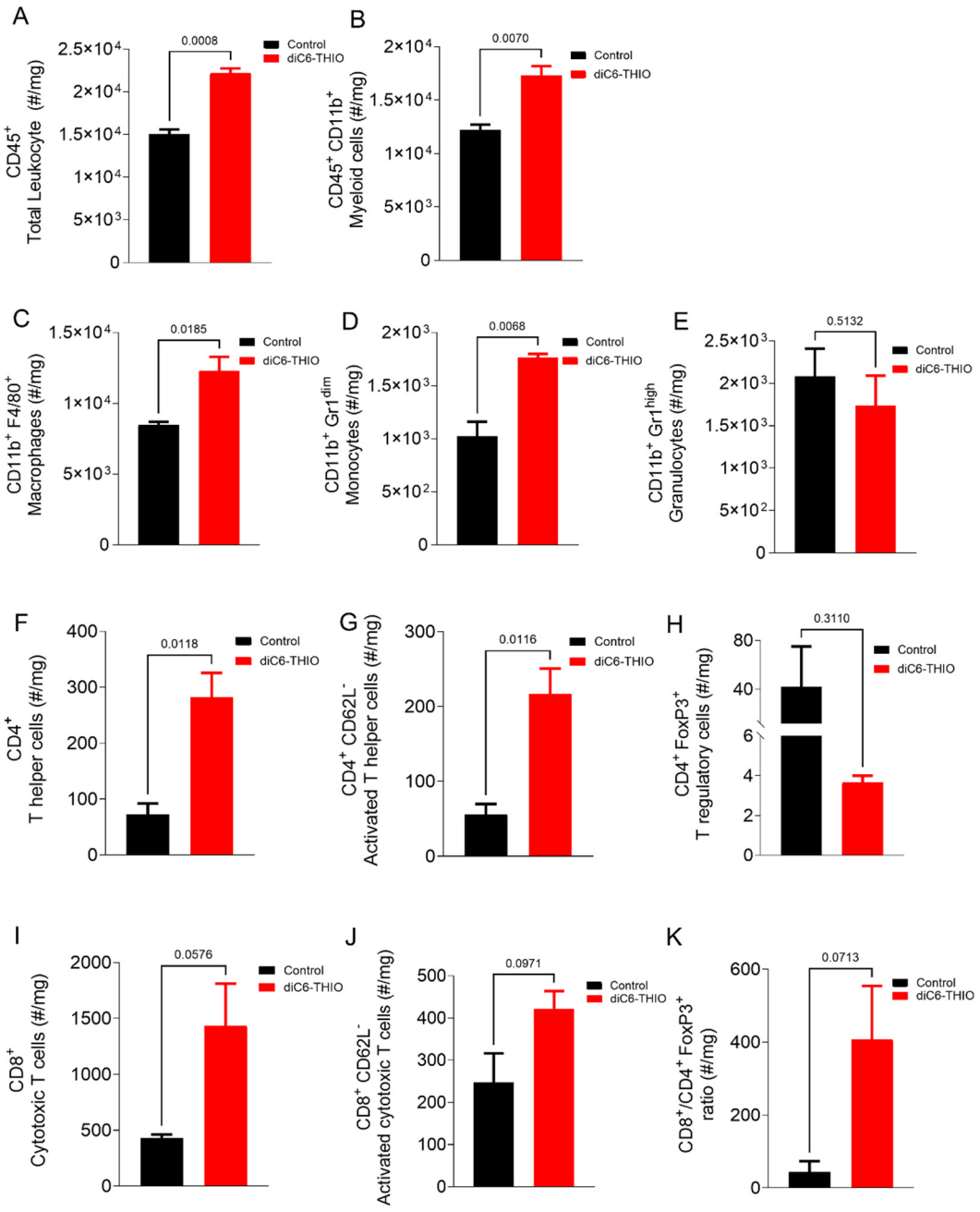

Figure 4. Immunophenotyping of CT26 bearing mice after diC6-THIO treatment. Total leukocyte (A) and myeloid (B)subpopulations. Myeloid subpopulations (C-E), Lymphocyte subpopulations (F-J), cytotoxic T cells/ T regulatory cells ratio (K) in tumor tissue (number of cells in tumor tissue(#)/mg). Data are shown as means ± SEM. *p* values were determined by unpaired student-t test by using GraphPad Prism. Among the infiltrated immune cells, the dominant population was myeloid subpopulations (A, B). Despite the lack of statistical significance among groups for $CD8^+$, $CD8^+$ $CD62L^-$, $CD8^+$ $CD4^+$ $FoxP3^+$ and $CD4^+$ $FoxP3^+$ panels ($p>0.05$), the trend for T helper and cytotoxic T cells were indicated that diC6-THIO has potential to induce activated T cell infiltration (F, G, I, J). Oppositely, in the treatment group, T regulatory cell numbers decreased (H). Following diC6-THIO treatment cytotoxic T cells: T regulatory cells ratio increased (K).

diC6-THIO Treatment Reduces Tumor Growth Compared to Control and Anti-PD-L1 Therapy

We evaluated the therapeutic efficacy of the diC6-THIO compound, the anti-PD-L1 antibody and the sequential therapy of diC6-THIO and anti-PD-L1 in a CT26-derived syngeneic mouse model. We measured tumor volumes until tumor sizes reached approximately 2500 mm^3. While there was

 doi:10.20944/preprints202409.2316.v1

no significant tumor growth inhibition with anti-PD-L1 as a monotherapy, diC6-THIO alone or with sequential treatment of diC6-THIO and anti-PD-L1 showed a significant difference compared to control with no noticeable animal weight loss (Figure 5A-C). There were statistically significant differences between control vs diC6-THIO (****$p<0.0001$), control vs diC6-THIO + anti-PD-L1 (****$p<0.0001$), diC6-THIO vs anti-PD-L1(***$p=0.0009$) and diC6-THIO +anti-PD-L1 vs anti-PD-L1 (***$p=0.0003$). No statistically significant difference was observed between diC6-THIO vs diC6-THIO + anti-PD-L1 and control vs anti-PD-L1. While no statistically significant difference was observed between the diC6-THIO and sequential therapy group, the trend suggests that the sequential therapy involving diC6-THIO and anti-PD-L1 holds the potential to decrease tumor volume. In addition, aspartate transaminase (AST) and alanine transaminase (ALT) plasma levels were evaluated for liver function (Supplementary Figure S4A) and creatinine, and urea nitrogen (BUN) plasma levels were evaluated for renal function (Supplementary Figure S4B). Even though treatment groups did not alter creatinine and BUN compared to control, ALT and AST levels were decreased in treatment groups compared to control.

 doi:10.20944/preprints202409.2316.v1

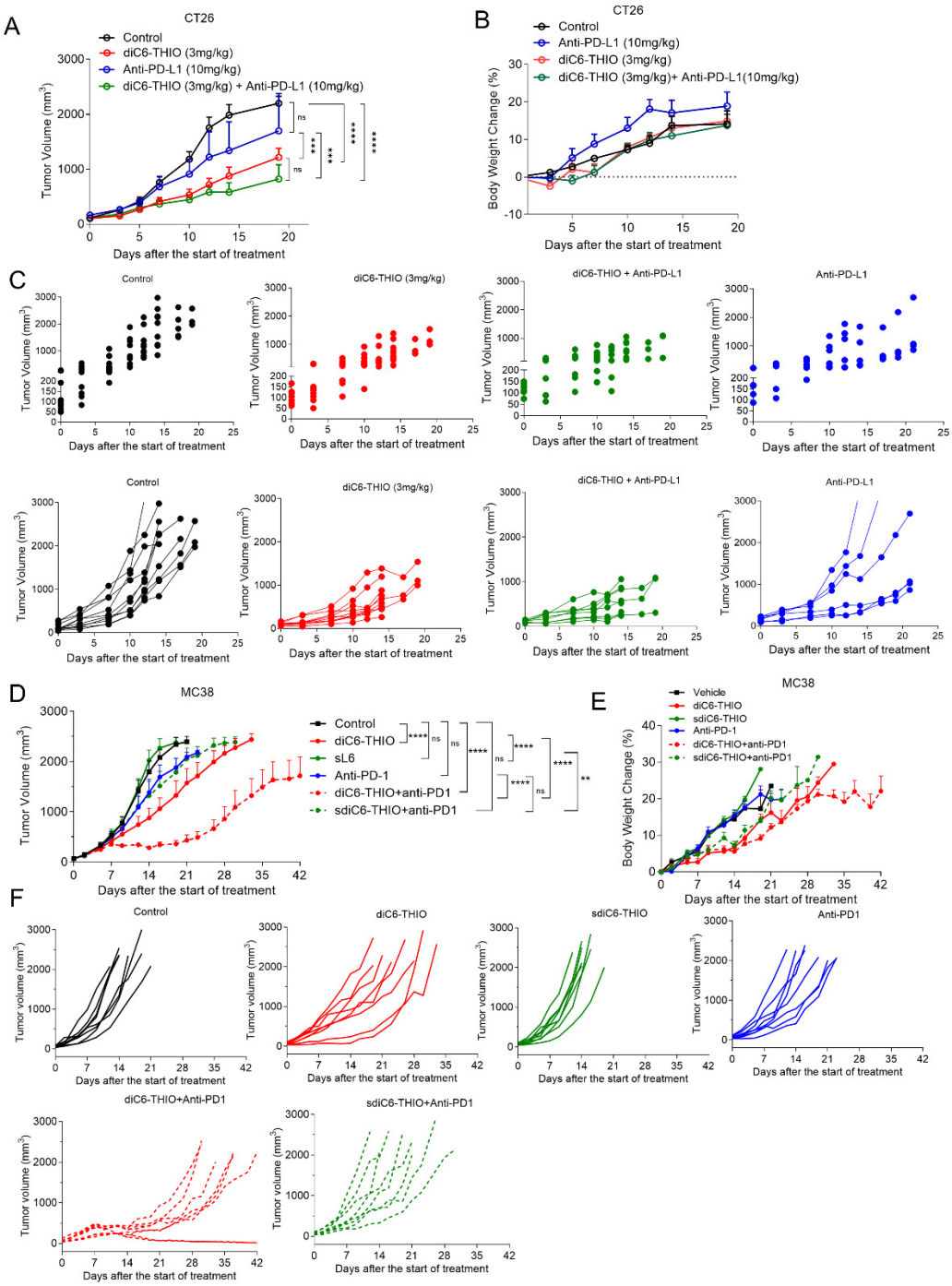

Figure 5. Therapeutic efficacy of diC6-THIO when sequentially combined with anti-PD-L1 in CT26 and MC38 colon cancer models. Data are shown as means ± SEM. *p* value was determined by two-way ANOVA by using Graphpad Prism. In the CT26 mouse model, the mice were administered with 3 mg/kg diC6-THIO (i.p) on days 0, 2, 7, 9 and/or 10mg/kg anti-PDL1 (i.p) on days 4, 11. there was statistically significant difference between control vs diC6-THIO (****p<0.0001), control vs diC6-THIO+anti-PD-L1 (****p<0.0001), diC6-THIO vs anti-PD-L1 (***p=0.0009) and diC6-THIO+anti-PD-L1 vs anti-PD-L1 (***p=0.0003). No significant differences were found between diC6-THIO vs diC6-THIO+anti-PD-L1 (p=0.3222) and control vs anti-PD-L1 (p=0.4222). For statistical purposes only, the final measurements from the euthanized mice were included up to the completion of each group, which occurred on day 19 (A). The body weight changes of mice in percentage from CT26 control, diC6-THIO, diC6-THIO+anti-PDL1 and anti-PDL1 groups (B). Individual CT26 tumor growth curves from control and treatment groups (C). In MC38 mouse model treatment groups, the mice were administered with 6 mg/kg diC6-THIO (i.v.) or 6 mg/kg sdiC6-THIO (i.v.) on days 0, 1, 2, 7, 8, 9 and/or

 doi:10.20944/preprints202409.2316.v1

10mg/kg anti-PD1 (i.p.) on days 4 and 12 (n=8 per group). There were statistically significant differences between control vs diC6-THIO (****p<0.0001), control vs diC6-THIO+anti-PD1 (****p<0.0001), diC6-THIO+ anti-PD1 vs anti-PD1 (****p<0.0001), control vs diC6-THIO+anti-PD1 (****p<0.0001), anti-PD1 vs DIC6-THIO + anti-PD1 (****p<0.0001), diC6-THIO vs diC6-THIO+anti-PD1 (****p<0.0001), sdiC6-THIO vs sdiC6-THIO + anti-PD1 (**p=0.0013), and diC6-THIO vs sdiC6-THIO (****p<0.0001). No significant differences (ns) were found between control vs sdiC6-THIO (p= 0.9301), control vs anti-PD1 (p=0.1357), control vs sdiC6-THIO+anti-PD1 (p=0.0756) and anti-PD1 vs sdiC6-THIO+anti-PD1 (p=0.9995). For statistical calculations, the final measurements from the euthanized mice are included until the completion of each group, which is determined by the endpoint reached when all mice in that group die. When comparing two groups, the statistical calculations consider the endpoint of the earlier group as reference (D). The body weight changes in percentage from MC38 control, diC6-THIO, sdiC6-THIO, diC6-THIO+ anti-PD1, sdiC6-THIO + anti-PD1 and anti-PD1 groups (E). Individual MC38 tumor growth curves from control and treatment groups (F).

We next evaluated the therapeutic efficacy of the active compound diC6-THIO and its metabolically more stable and inactive control form, designated as sdiC6-THIO, in a MC38-derived syngeneic mouse model. While diC6-THIO contains natural phosphodiester (P-O) linkage, where it connects the fatty acid residues of the lipid groups to 6-thio-dG, sdiC6-THIO contains enzymatically more stable non-natural modified phosphorothioate (P-S) linkage (Supplementary Figure S5A). The specific chemical nature of the P-S linkage makes this compound more stable in cells; thus, the nucleoside pharmacophore - 6-thio-dG is not readily released from the sdiC6-THIO prodrug in cells. Cell viability assays of MC38 and LLC cells confirmed the differences in biological activity of these compounds in vitro. Two independent in vitro experiments conducted in MC38, and LLC cells showed 14-120-fold difference in activity between diC6-THIO and sdiC6-THIO (Supplementary Figure S5B,C). When we compared the compounds' efficacies in vivo, we found significant tumor growth delay with diC6-THIO alone. However, its metabolically less active form sdiC6-THIO did not show any therapeutic effect compared to PBS treated controls. In addition, we compared diC6-THIO and sdiC6-THIO treated animals to their ICI combinational counterparts – groups with sequential treatments of diC6-THIO and anti-PD1, or sdiC6-THIO and anti-PD1 agent. Sequential treatment with diC6-THIO and anti-PD1 compounds showed significant differences when compared to control, diC6-THIO alone, and anti-PD1 alone, without noticeable animal weight loss. Sequential treatment with sdiC6-THIO and anti-PD1 did not show significant differences when compared to control or anti-PD1 agents alone. Sequential treatment with sdiC6-THIO and anti-PD1 had significant differences when compared to sdiC6-THIO alone (Figure 5D-F).

We also evaluated the therapeutic efficacy of diC6-THIO and sdiC6-THIO in a different cancer model. We selected LLC cell-based murine lung cancer model and confirmed the similar therapeutic effects of diC6-THIO in this alternative model. Once again, we lost the therapeutic efficacy when we used the inactive sdiC6-THIO form of the molecule. The sequential administration of diC6-THIO and anti-PD1 resulted in significant differences in the LLC model when compared to diC6-THIO or anti-PD1 groups alone. The sequential treatment of sdiC6-THIO and anti-PD1 did not show significant differences when compared to sdiC6-THIO or anti-PD1 alone (Supplementary Figure S5D-F). These results indicate that hydrolytically less stable P-O intermodular linkage allows for the release of 6-thio-dG from the prodrug and provides for therapeutic activity. Additionally, diC6-THIO combination with anti-PD1 agent provides additional therapeutic efficacy not only in colorectal, but also in lung cancer models.

4. Discussion

Various drug delivery systems have been developed to enhance cellular uptake to achieve high drug accumulation to improve cancer treatment outcomes. Chemotherapies, due to the insufficient target cancer cell specificity, cause toxicity in healthy tissues, and thus, limit their therapeutic efficiency. To overcome these obstacles, the prodrug approaches have evolved to achieve tumor-specific drug delivery and reduce toxic side effects [28].

 doi:10.20944/preprints202409.2316.v1

In previous studies, a phospholipid-doxorubicin conjugate showed high drug loading content and facilitated cell internalization [29]. Another study also showed the successful conjugation of fatty acid, squalenoic acid (SQ) to gemcitabine, paclitaxel, doxorubicin, and adenosine [30-33]. Sauraj et al. [34] designed an effective delivery approach for 5-fluorouracil based on xylan-stearic acid conjugates and showed higher cellular apoptosis in vitro in colorectal cancer cells, thus showing the advantages of small lipid prodrugs-based drug delivery systems. Deoxycytidine analog gemcitabine has a short circulation half-life due to metabolic instability, and poor diffusion into tumor cells due to drug resistance development and its hydrophilic moieties. Wu et al. [35] developed a prodrug with PUFAylation technology that contains gemcitabine, and hydrophobic linoleic acid via amide linkage. This study showed that gemcitabine was protected from rapid deactivation by cytidine deaminase and increased in vitro cytotoxicity in L3.6pl and BXPC-3 pancreatic cancer cells compared to non-conjugated gemcitabine.

Here, we designed and evaluated a series of new phosphatidyl-lipid-modified nucleoside conjugated bimodular molecules. We evaluated various cancer cell lines, including metastatic derivatives, to compare their responses to the dihexanoyl phosphatidyl derivative of 6-thio-dG, referred to as diC6-THIO. We demonstrated that metastatic cells derived from MDAMB-231 exhibit increased telomerase activity, as assessed by the ddTRAP assay [22], and show increased sensitivity to diC6-THIO treatment. The ddTRAP assay demonstrates that elevated telomerase activity increases cellular sensitivity to both 6-thio-dG and diC6-THIO. This observation is further supported by the EC_{50} data, which show that BrM and BoM cells, characterized by higher telomerase activity, exhibit greater sensitivity to both compounds. Overall, there was little difference in sensitivity between diC6-THIO and 6-thio-dG across these cell types. However, these results indicate that other tumor types are very sensitive to both compounds. Since diC6-THIO is more soluble compared to 6-thio-dG, this is a significant advantage to progress diC6-THIO in additional pre-clinical and in the future into clinical trials. After evaluating the EC_{50} values across different cell lines, we selected colorectal cancer cell lines for in vivo studies, as diC6-THIO demonstrated enhanced anticancer activity in these cells and exhibited improved solubility in aqueous biological media. Phospholipid conjugated prodrugs typically have a therapeutic agent, a phosphate group, and a glycerol residue esterified with fatty acids as their main components. The diC6-THIO molecule also consists of 6-thio-dG as a telomerase-dependent telomere-targeting pharmacophore, a phosphate group linker and hexanoyl diglyceride as the main compound structural components. Telomere-targeting activity of diC6-THIO is associated with the induction of enhanced telomere damage (TIFs), which is one of the most accurate pharmacodynamic markers of the compound mechanism of action and on-target activity indicator. Since human telomeres are only about 1/6000th of the entire genome, damage to telomeres only rarely occurs. We employed a novel ImageJ-based technique, called DiAna, capable of conducting spatial analysis in three dimensions to calculate the spatial separation between co-localized object volumes for every selected pair of objects (Supplementary Figure S1B). Co-localization analysis is performed using a pixel-based method [36, 37], an object-based method [38-40], or a hybrid approach that integrates both techniques [41]. In the pixel-based approach, co-localization analysis is affected by the inherent noise of fluorescent images and lacks the ability to provide spatial information concerning the relationship between objects. Meanwhile, object-based approaches have limitations as the threshold is globally applied to the whole image. Within the DiAna tool, we implemented 3D segmentation analysis and demonstrated precise and robust object extraction despite variations in object size and intensity across the images. The segmentation facilitates the precise calculation of the spatial volume occupied by an object in 3D space, along with the determination of the object's geometric centroid or center of mass. Notably, this method effectively circumvents the inherent biases associated with 2D image analysis. The advantages of this method include its reduced susceptibility to actual pixel intensity values, robustness in handling background noise, and its freedom from dependence on arbitrarily defined intensity threshold values. Using this analysis method, we found that diC6-THIO induces more TIFs formation compared to the unconjugated parent pharmacophore 6-thio-dG. This indicates a potential role for the lipid conjugated group in targeting telomeres, more efficiently in telomerase positive cells.

 doi:10.20944/preprints202409.2316.v1

Moreover, diC6-THIO was evaluated in combination with radiation therapy in HT29 colorectal cancer cells in vitro. Pretreatment with diC6-THIO for 24h followed by radiation therapy resulted in increased toxicity compared to treatment with diC6-THIO or radiation therapy alone at both 2 Gy and 4Gy doses of ionizing radiation (Supplementary Figure S6A,B).

In cancer, intrinsic sensing deficits restrict T cell activation in the tumor microenvironment. Hence, innovative approaches and therapeutic agents are needed for combination therapies targeting patients both innate and adaptive immune systems to overcome this limitation. Currently, PD-1/PD-L1 blockade benefits are limited and require additional therapy, or novel compounds and their combinations to overcome anti-PD-L1 agents' resistance. Our in vivo immunophenotyping data showed that diC6-THIO treatment noticeably elevated tumor infiltration of activated T cells, while diminishing Treg cells in tumor tissues. Moreover, the cytotoxic T cells/ Treg cells ratio was increased by administration of diC6-THIO treatment, where cytotoxic T cells serve as the anticancer efficacy indicator. In our studies, infiltration of immune cells was enhanced into the tumor microenvironment that is consistent with the decrease in tumor volumes following diC6-THIO treatment. These results indicate the potential clinical benefit of diC6-THIO alone or in combination with immune checkpoint inhibitors in colorectal cancer patients.

Taken together, our results demonstrate that the direct telomerase-mediated telomere-targeted anti-cancer effects for the bimodular prodrug 6-thio-dG-lipid-conjugate (diC6-THIO) is more pronounced than those for the unconjugated nucleoside pharmacophore in colorectal cancer models. In conclusion, we have introduced a new telomerase-mediated telomere-targeted glycerophospholipid-based prodrug that holds promise for a high anticancer therapeutic efficacy in vivo. Anticancer activity of this class of telomere-modifying prodrugs should be evaluated further in various other tumor xenograft and syngeneic mouse models.

5. Conclusions

We demonstrated potent and specific anticancer activity of a novel telomerase activity-dependent telomere-targeting small molecule, diC6-THIO. The compound is effective in telomerase-expressing cancer cells, but not in normal telomerase negative fibroblasts. One of the most active molecules from this class of conjugates-diC6-THIO induces more telomeric DNA damage and higher anti-cancer activity. Importantly, this compound has high solubility in aqueous media in comparison with the parental 6-thio-dG compound, currently in phase II clinical trials for lung cancer. Our findings in colorectal cancer models provide important proof-of-principle results demonstrating the efficacy of diC6-THIO both in vitro and in vivo. Furthermore, we show that diC6-THIO treatment increases the proportion of infiltrated immune cells within the tumor microenvironment, and thus has a good potential to increase general therapeutic responses to immunotherapies for colorectal cancer treatment.

Supplementary Materials: The following supporting information can be downloaded at the website of this paper posted on Preprints.org.

Author Contributions: Conceptualization, M.Y., Z.G.D.,I.M.,S.M.G. and J.W.S.; methodology, M.Y., Z.G.D.,I.M.,S.M.G. and J.W.S; software, S.E.E.; validation, M.Y.,S.G.,G.E., S.E.E, Z.G.D., I.M., S.M.G. and J.W.S.; formal analysis, M.Y., S.G., S.E.E., G.E. Z.G.D., I.M., S.M.G. and J.W.S.; investigation, M.Y., S.G., A.K.T. and A.A.; resources, S.M.G. and L.L.B.; data curation, M.Y., S.G.; writing—original draft preparation, M.Y., Z.G.D.; writing—review and editing, M.Y., Z.G.D., I.M., S.E.E., S.M.G. and J.W.S; visualization, M.Y., S.G. and I.M.; supervision, Z.G.D and J.W.S.; funding acquisition, S.M.G and Z.G.D. All authors have read and agreed to the published version of the manuscript.

Funding: This research was funded by "MAIA Biotechnology," "Hacettepe University Scientific Research Projects Coordination Unit" and NIH grant C06 RR30414, CA142543, and CA070907 to J.W.S. who holds the Southland Foundation Distinguished Chair in Geriatrics.

Institutional Review Board Statement: This study adheres to the highest ethical standards in research involving animals. All animal experiments were conducted in strict accordance with the guidelines provided by KOBAY

DLH A.S., and the protocol was approved by the Hacettepe University institutional ethics committee (protocol code 603, 02/04/2022).

Data Availability Statement: The datasets generated during and/or analyzed during the current study are available from the corresponding author on reasonable request.

Acknowledgments: We thank Romina Girotti for her expert editorial assistance during the preparation of the manuscript.

Conflicts of Interest: Sergei M. Gryaznov is the chief scientific officer, Jerry W. Shay is a scientific advisor, Z. Gunnur Dikmen is a scientific advisor, and Ilgen Mender is a director of Biology Research at MAIA Biotechnology. The remaining authors have no conflict of or competing interest to declare.

References

1. Siegel, R.L., et al., Cancer statistics, 2023. CA Cancer J Clin, 2023. 73(1): p. 17-48.
2. Kuipers, E.J., et al., Colorectal cancer. Nat Rev Dis Primers, 2015. 1: p. 15065.
3. Johdi, N.A. and N.F. Sukor, Colorectal Cancer Immunotherapy: Options and Strategies. Front Immunol, 2020. 11: p. 1624.
4. Marcus, L., et al., FDA Approval Summary: Pembrolizumab for the Treatment of Microsatellite Instability-High Solid Tumors. Clin Cancer Res, 2019. 25(13): p. 3753-3758.
5. Jacome, A.A. and C. Eng, Role of immune checkpoint inhibitors in the treatment of colorectal cancer: focus on nivolumab. Expert Opin Biol Ther, 2019. 19(12): p. 1247-1263.
6. Li, J. and X. Xu, Immune Checkpoint Inhibitor-Based Combination Therapy for Colorectal Cancer: An Overview. Int J Gen Med, 2023. 16: p. 1527-1540.
7. Giang, I., E.L. Boland, and G.M. Poon, Prodrug applications for targeted cancer therapy. AAPS J, 2014. 16(5): p. 899-913.
8. Walther, R., J. Rautio, and A.N. Zelikin, Prodrugs in medicinal chemistry and enzyme prodrug therapies. Adv Drug Deliv Rev, 2017. 118: p. 65-77.
9. Fattahi, N., et al., Emerging insights on drug delivery by fatty acid mediated synthesis of lipophilic prodrugs as novel nanomedicines. J Control Release, 2020. 326: p. 556-598.
10. Dahan, A., et al., The prospects of lipidic prodrugs: an old approach with an emerging future. Future Med Chem, 2019. 11(19): p. 2563-2571.
11. Mura, S., et al., Lipid prodrug nanocarriers in cancer therapy. J Control Release, 2015. 208: p. 25-41.
12. Sreekanth, V. and A. Bajaj, Recent Advances in Engineering of Lipid Drug Conjugates for Cancer Therapy. ACS Biomater Sci Eng, 2019. 5(9): p. 4148-4166.
13. Irby, D., C. Du, and F. Li, Lipid-Drug Conjugate for Enhancing Drug Delivery. Mol Pharm, 2017. 14(5): p. 1325-1338.
14. Huang, L., et al., Engineering of small-molecule lipidic prodrugs as novel nanomedicines for enhanced drug delivery. J Nanobiotechnology, 2022. 20(1): p. 49.
15. Griffith, J.D., et al., Mammalian telomeres end in a large duplex loop. Cell, 1999. 97(4): p. 503-14.
16. Blackburn, E.H., Structure and function of telomeres. Nature, 1991. 350(6319): p. 569-73.
17. Shay, J.W. and W.E. Wright, Telomerase: a target for cancer therapeutics. Cancer Cell, 2002. 2(4): p. 257-65.
18. Shay, J.W. and S. Bacchetti, A survey of telomerase activity in human cancer. Eur J Cancer, 1997. 33(5): p. 787-91.
19. Mender, I., S. Gryaznov, and J.W. Shay, A novel telomerase substrate precursor rapidly induces telomere dysfunction in telomerase positive cancer cells but not telomerase silent normal cells. Oncoscience, 2015. 2(8): p. 693-5.
20. Mender, I., et al., Induction of telomere dysfunction mediated by the telomerase substrate precursor 6-thio-2'-deoxyguanosine. Cancer Discov, 2015. 5(1): p. 82-95.
21. Gilles, J.F., et al., DiAna, an ImageJ tool for object-based 3D co-localization and distance analysis. Methods, 2017. 115: p. 55-64.
22. Ludlow, A.T., et al., Quantitative telomerase enzyme activity determination using droplet digital PCR with single cell resolution. Nucleic Acids Research, 2014. 42(13): p. e104-e104.
23. Zhang, J., et al., Enrichment and characterization of cancer stem-like cells in ultra-low concentration of serum and non-adhesive culture system. Am J Transl Res, 2018. 10(5): p. 1552-1561.
24. Zhong, Y., et al., Spheres derived from the human SK-RC-42 renal cell carcinoma cell line are enriched in cancer stem cells. Cancer Lett, 2010. 299(2): p. 150-60.
25. Godoy, P., et al., Recent advances in 2D and 3D in vitro systems using primary hepatocytes, alternative hepatocyte sources and non-parenchymal liver cells and their use in investigating mechanisms of hepatotoxicity, cell signaling and ADME. Archives of Toxicology, 2013. 87(8): p. 1315-1530.

 doi:10.20944/preprints202409.2316.v1

26. Boudreau, N., Z. Werb, and M.J. Bissell, Suppression of apoptosis by basement membrane requires three-dimensional tissue organization and withdrawal from the cell cycle. Proc Natl Acad Sci U S A, 1996. 93(8): p. 3509-13.
27. Mender, I., et al., Activating an Adaptive Immune Response with a Telomerase-Mediated Telomere Targeting Therapeutic in Hepatocellular Carcinoma. Mol Cancer Ther, 2023. 22(6): p. 737-750.
28. Delahousse, J., C. Skarbek, and A. Paci, Prodrugs as drug delivery system in oncology. Cancer Chemother Pharmacol, 2019. 84(5): p. 937-958.
29. Wang, H., et al., Doxorubicin conjugated phospholipid prodrugs as smart nanomedicine platforms for cancer therapy. J Mater Chem B, 2015. 3(16): p. 3297-3305.
30. Bui, D.T., et al., Multifunctional squalene-based prodrug nanoparticles for targeted cancer therapy. Chem Commun (Camb), 2014. 50(40): p. 5336-8.
31. Emamzadeh, M., et al., Dual controlled delivery of squalenoyl-gemcitabine and paclitaxel using thermo-responsive polymeric micelles for pancreatic cancer. J Mater Chem B, 2018. 6(15): p. 2230-2239.
32. Mougin, J., et al., Stacking as a Key Property for Creating Nanoparticles with Tunable Shape: The Case of Squalenoyl-Doxorubicin. ACS Nano, 2019. 13(11): p. 12870-12879.
33. Gobeaux, F., et al., Albumin-driven disassembly of lipidic nanoparticles: the specific case of the squalene-adenosine nanodrug. Nanoscale, 2020. 12(4): p. 2793-2809.
34. Sauraj, et al., Lipophilic 5-fluorouracil prodrug encapsulated xylan-stearic acid conjugates nanoparticles for colon cancer therapy. Int J Biol Macromol, 2019. 128: p. 204-213.
35. Wu, L., et al., Self-Assembled Gemcitabine Prodrug Nanoparticles Show Enhanced Efficacy against Patient-Derived Pancreatic Ductal Adenocarcinoma. ACS Appl Mater Interfaces, 2020. 12(3): p. 3327-3340.
36. Li, Q., et al., A syntaxin 1, Galpha(o), and N-type calcium channel complex at a presynaptic nerve terminal: analysis by quantitative immunocolocalization. J Neurosci, 2004. 24(16): p. 4070-81.
37. Manders, E.M., et al., Dynamics of three-dimensional replication patterns during the S-phase, analysed by double labelling of DNA and confocal microscopy. J Cell Sci, 1992. 103 (Pt 3): p. 857-62.
38. Lachmanovich, E., et al., Co-localization analysis of complex formation among membrane proteins by computerized fluorescence microscopy: application to immunofluorescence co-patching studies. J Microsc, 2003. 212(Pt 2): p. 122-31.
39. Obara, B., et al., A novel method for quantified, superresolved, three-dimensional colocalisation of isotropic, fluorescent particles. Histochem Cell Biol, 2013. 139(3): p. 391-402.
40. Bolte, S. and F.P. Cordelieres, A guided tour into subcellular colocalization analysis in light microscopy. J Microsc, 2006. 224(Pt 3): p. 213-32.
41. Jaskolski, F., C. Mulle, and O.J. Manzoni, An automated method to quantify and visualize colocalized fluorescent signals. J Neurosci Methods, 2005. 146(1): p. 42-9.